ADVANCED MATERIALS
www.advmat.de

Self-Assembly of Large-Area 2D Polycrystalline Transition Metal Carbides for Hydrogen Electrocatalysis

Xining Zang, Wenshu Chen, Xiaolong Zou, J. Nathan Hohman, Lujie Yang, Buxuan Li, Minsong Wei, Chenhui Zhu, Jiaming Liang, Mohan Sanghadasa, Jiajun Gu,* and Liwei Lin**

Low-dimensional (0/1/2 dimension) transition metal carbides (TMCs) possess intriguing electrical, mechanical, and electrochemical properties, and they serve as convenient supports for transition metal catalysts. Large-area single-crystalline 2D TMC sheets are generally prepared by exfoliating MXene sheets from MAX phases. Here, a versatile bottom-up method is reported for preparing ultrathin TMC sheets (≈10 nm in thickness and >100 µm in lateral size) with metal nanoparticle decoration. A gelatin hydrogel is employed as a scaffold to coordinate metal ions (Mo^{5+}, W^{6+}, Co^{2+}), resulting in ultrathin-film morphologies of diverse TMC sheets. Carbonization of the scaffold at 600 °C presents a facile route to the corresponding MoC_x, WC_x, CoC_x, and to metal-rich hybrids ($Mo_{2-x}W_xC$ and W/Mo_2C–Co). Among these materials, the Mo_2C–Co hybrid provides excellent hydrogen evolution reaction (HER) efficiency (Tafel slope of 39 mV dec^{-1} and 48 $mV_{j = 10\ mA\ cm^{-2}}$ in overpotential in 0.5 M H_2SO_4). Such performance makes Mo_2C–Co a viable noble-metal-free catalyst for the HER, and is competitive with the standard platinum on carbon support. This template-assisted, self-assembling, scalable, and low-cost manufacturing process presents a new tactic to construct low-dimensional TMCs with applications in various clean-energy-related fields.

The clean combustion of hydrogen has presented an attractive alternative to fossil fuel use.[1,2] Considerable improvements in hydrogen fuel-cell technology and solid-state hydrogen storage have made significant strides in recent years.[3,4] Electrocatalytic hydrogen evolution using sustainably produced electricity has promised a carbon-free production of a chemical fuel.[5] However, most commercial hydrogen is still produced via steam reforming of methane because there are few scalable base-metal replacements for platinum at the scales required for electrocatalysis.[6] Dimensional reduction of 3D materials to 0D, 1D, or 2D nanostructures (thickness vs lateral size < 1%),[7,8] has attracted interest for discovering intriguing new catalytic properties. Notably, including 2D nanostructures comprised of metals,[9] transition metal dichalcogenides,[10–12] transition metal oxides,[13,14] and 2D transition metal carbides (TMCs)[15] have been explored for enhanced catalytic performance, and advances in this area have led to reliable and cost-effective fabrication methods ideal for base-metal hydrogen evolution catalysts.

Among these materials, 2D TMCs possess excellent electrical conductivity, electrochemical activity, high surface area, and strong chemical resilience.[16] These make them particularly desirable for various clean energy applications such as energy storage[17–19] and catalysis.[7,15] The most widely applied method toward 2D TMCs requires a selective etching process from their

Dr. X. Zang
Research Laboratory of Electronics
Massachusetts Institute of Technology
Cambridge, MA 02139, USA
E-mail: xzang@mit.edu
Dr. X. Zang, L. Yang, B. Li, Dr. M. Wei, Prof. L. Lin
Mechanical Engineering
University of California Berkley
Berkeley, CA 94704, USA
E-mail: lwlin@berkeley.edu
W. Chen, Prof. J. Gu
State Key Laboratory of Metal Matrix Composites
Shanghai Jiao Tong University
Shanghai 200240, China
E-mail: gujiajun@sjtu.edu.cn
Prof. X. Zou, J. Liang, Prof. L. Lin
Tsinghua–Berkeley Shenzhen Institute
Shenzhen 518055, China
Dr. J. N. Hohman
The Molecular Foundry
Lawrence Berkeley National Lab
Berkeley, CA 94704, USA
Dr. C. Zhu
Advanced Light Source
Lawrence Berkeley National Lab
Berkeley, CA 94704, USA
Dr. M. Sanghadasa
U.S. Army RDECOM AMRDEC
Redstone Arsenal
AL 35898, USA
The ORCID identification number(s) for the author(s) of this article can be found under https://doi.org/10.1002/adma.201805188.

DOI: 10.1002/adma.201805188

ternary MAX phases[20] ($M_{n+1}AX_n$, M is transition metal, A is a group 12–16 elements, and X is C or N)[21,22] using fluoride-based etching solutions to selectively remove the element "A" from a MAX crystal.[23] Fluoride-free methods for preparing 2D TMCs have been reported, notably chemical vapor deposition (CVD) on metal foils or graphene but the reported yield is extremely low.[8,24,25] Therefore, developing a robust and versatile fabrication method for 2D TMCs is required to enable practical applications and large-scale manufacturing.

The assembly of metal ions and peptides into nanostructured materials has been known since the 1950s.[26,27] The process parameters (concentration, peptide selection, and temperature) can be carefully controlled to enable the preparation of hydrogel materials containing 0D particles, 1D tubes, or 2D lamellar products.[28,29] These self-assembling soft structures are amenable to subsequent transformation by thermal and chemical approaches.[9] By selecting carbide-forming metals, a nanostructured hydrogel can be prepared that is amenable for subsequent conversion into TMCs that retain their supramolecular dimensionality. When a hydrogel with embedded transition metal ions is heated, self-accumulation of polymeric phases of metal carbide degradation products occurs at the hydrogel air/liquid interface in a process described by the buoyancy–Marangoni effect (**Figure 1**a–d).[30–32] The self-assembly and ordering of gelatin can therefore macroscopically arrange precursors into structures that can be collapsed into dimensionally conserved nanostructures.[33,34]

Here, we demonstrate the synthesis of metallohydrogels and their subsequent carbonization into ultrathin metal-carbide nanostructures (2D TMCs) (Figure 1a–e). Hydrogel membranes serve as templates to constrain the conversion of metal ions to form ultrathin 2D (extremely low aspect ratio) large-area polycrystalline carbide nanosheets. Various ion–gel systems are carbonized in this way, yielding Mo_2C, W_2C, and Co_3C (Figure 1f–h), with up to ≈100 µm lateral size. Moreover, using this self-assembly scheme, we are able to synthesize Mo_2C structures decorated by Co nanoparticles, which provides superior hydrogen evolution reaction (HER) performance (Tafel slope of 39 mV dec^{-1} and overpotential of 48 $mV_{j=10\ mA\ cm^{-2}}$ in 0.5 M H_2SO_4, which is comparable to commercial Pt/C. Our results show that collapsible scaffolds can be used to prepare earth-abundant transition-metal hydrogen evolution catalysts with performance competitive with noble-metal-based platinum on carbon standard.

Figure 1 shows a hierarchical overview of the collapsible hydrogel and its subsequent conversion to 2D-TMC nanosheets. Metal precursor is well assembled in the metallohydrogel as gelatin-immobilized metal complexes, utilizing the protein triple helix structure decorated with a large number of functional groups (such as amide, amino, hydroxyl, carboxyl groups, etc.).[35,36] Supramolecular self-organization is driven by transition metal complexes' addition to a solution of gelatin. Each supramolecular complex is named by the associated metal, (Mo–gelatin, W–gelatin, or Co–gelatin). Weak coordination

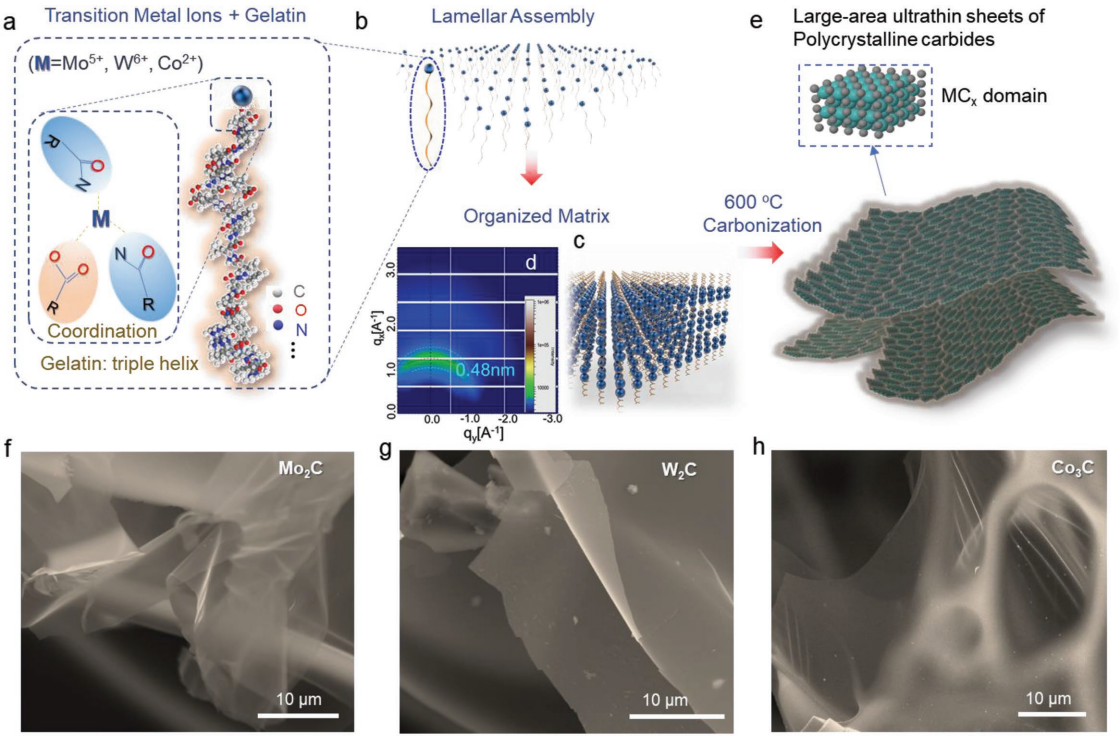

Figure 1. Self-assembly process for large-area ultrathin 2D TMCs. a) Transition metal ions such as Mo^{5+}, W^{6+}, Co^{2+} are mixed in the gelatin-mediated hydrogel with rich functional groups as ligands. b,c) Under an elevated temperature, the ion–gelatin solution takes (b) a lamellar assembly process that results in (c) a layer-by-layer organized matrix. d) GIWAXS of Mo–gelatin template as an example to show that gelatin constrains the metal ions laterally between the layers. e) Carbonized in a CH_4/H_2 atmosphere above 600 °C, the gelatin templates constrain the conversion of metal ions laterally between the layers, forming nanocrystalline 2D TMCs. CH_4 was used here to increase the carbon content and H_2 was used to suppress oxidations. f–h) SEM images of the resulting ultrathin 2D TMCs of (f) Mo_2C, (g) W_2C, and (h) Co_3C flakes, respectively.

between metal complexes and the long, amphiphilic gelatin strands tends to drive phase segregation into lamellar phases (Figure 1b,c). A high concentration (2 m, molal, mol kg^{-1} solvent) of the transition metal complex ensures that there is sufficient precursor to form the target nanostructures after carbonization.

Films of the metal–gelatin structures are examined by grazing-incidence wide-angle X-ray scattering (GIWAXS), and shown in Figure 1d. The diffuse bands at between 1 and 1.5q are consistent with long range order in the metallohydrogels and moderate preferential orientation of lamellar phases normal to the surface. The central peak at ≈1.25q corresponds to a 0.48 nm interlayer spacing. We also performed a study of gelatin concentration and addition of organic solvents and surfactants. The results are summarized in the Supporting Information, showing that adding alcohol in aqueous metallogel induce a broad subpeak, indicating an accumulation layer distance of 0.78 nm. The W–gel dissolved in the organic solvent *N*-methyl-2-pyrrolidone (NMP) exhibits a larger lamellar spacing of 1.29 nm (Figure S1, Supporting Information).

Carbonization at 600 °C in a reducing H_2/CH_4 environment from the ordered matrix (Figure 1c) to the 2D TMC is shown schematically in Figure 1e. The M–gelatin structures were prepared using a relatively high concentration of metal ions (2 m, molal), and a firm hydrogel was found to yield ideal substrates for conversion (>30 wt% gelatin). Mo^{5+} and W^{6+} with high positive charge and near empty d-orbital can coordinate with amino acid groups in gelatin effectively.[37] WCl_6 and $CoSO_4$ were dissolved in NMP and deionized (DI) water (2 M) with 60 wt% gelatin, respectively. Lower concentrations of gelatin (<10 wt%) gave poor conversion and generally yielded metal oxides. While gelatin provides a considerable amount of carbon for the conversion to the metal carbide, pure argon gas yielded incomplete conversion. A reducing environment including H_2 and CH_4 was found to promote complete conversion and suppresses oxidation (Figure S2, Supporting Information).

The low-temperature synthesis process generated similar nanostructured materials regardless of metal ion. Scanning electron microscopy (SEM) images of Mo_2C, W_2C, and Co_3C derived from Mo^{5+}, W^{6+}, or Co^{2+} ions, respectively, are collected in Figure 1f–h. We postulate that the supramolecular 2D arrangement of the hydrogel helps lower the formation energy of both Mo_2C or W_2C, making them accessible at lower temperatures (600 °C) than previous reports for carbonization of TMCs or MXenes (at 1600 °C[20]).

Transmission electron microscopy (TEM) images of the carbonization products are shown in **Figure 2**a–c. Large polycrystalline ultrathin sheets of Mo_2C composed of nanocrystalline domains are roughly measured as ≈5 nm in size from TEM images, while using Scherrer equation, the lattice crystalline is ≈8 nm from X-ray diffraction (XRD) in Figure S2 (Supporting Information).[38] After the separation of these products by ultrasonication, we deposited them on silicon surfaces. Figure 2d shows atomic force microscopy (AFM) mapping results that reveal flat surfaces with a roughness of 0.22 ± 0.01 nm (Figure S3a–c, Supporting Information) and a nominal thickness of ≈10 nm. GIWAX diffraction patterns (Figure 2e and Figure S3d (Supporting Information)) show a preferred *z*-directional orientation and sublayer thicknesses of 2.4 and 1.6 nm. These characterizations support the expectation that the 2d-ordering of metal complexes within self-assembling M–gelatin supramolecular scaffold is conserved after carbonization. As expected for a metal carbide, the as-synthesized ultrathin β-Mo_2C has excellent thermal stability under 550 °C (see thermal gravimetric analysis (TGA), Figure S4, Supporting Information), whereas the widely reported $Ti_3C_2T_x$ MXene suffers from oxidation above 200 °C because of its rich surface terminations (T_x, such as OH/COOH groups) originating from selective etching process.[39]

As shown in the XRD spectra (Figure 2h), Mo_2C flakes have the same peaks of the $Mo_{2-x}W_xC$ flakes. This is because samples of Mo_2C and W_2C have similar crystalline structures ($P63/mm$), and both the samples exhibit intense reflections at {100}, {002}, and {101}. The multiple-layer, ultrathin 2D structure further helps reduce the processing time to <1/2 h, which is crucial for the large-scale production and low-cost manufacturing. It should be noted, however, further reducing the process temperature below 600 °C can yield α-MoC_{1-x} that are not desirable by water hydrolysis reactions (Figure S5, Supporting Information).

Interestingly, it is found that the synthesized Co_3C sheets have lots of well spread Co nanoparticles as the holding capacity of Co^{2+} in the gelatin matrix is lower than that of Mo^{5+} and W^{6+} due to the lower charge of Co. This makes extra Co^{2+} ions leave from the gelatin template, accumulate and form converted nanoparticles on the carbide framework (Figure 1e). This solution-based self-assembly process can also synthesize many large-scale ultrathin 2D hybrid structures. For example, mixing Mo^{5+} and W^{6+} ions together in the gelatin media yielded a hybrid of Mo_2C–W_2C after calcination (Figure 2f). In addition, by adding Co^{2+} ions in the gelatin mixture, Co nanoparticles reduced and were found deposited on the Mo_2C and W_2C thin flakes (Figure 2g and Figure S5a (Supporting Information)). Similarly, in a triple ion assembly process, $Mo_{2-x}W_xC$ flakes decorated with cobalt nanoparticles were synthesized by combining all three metals (Mo–W–Co) into the gelatin media (Figure S5b, Supporting Information). Detailed energy dispersive X-ray spectroscopy (EDS) and X-ray photoelectron spectroscopy (XPS) analyses for these materials are provided in Figures S6 and S7 (Supporting Information). GIWAX of $Mo_{2-x}W_xC$ is compared to Mo_2C, resolving <1% lattice strain (Figure S8, Supporting Information).

The HER performance of the as-grown β-Mo_2C is evaluated with different mass loadings of carbide catalyst on carbon paper (Figure S9, Supporting Information). We use platinum on carbon support (Pt/C)—a well-understood and effective HER catalyst, as a control sample. It is applied with the same mass loading in 0.5 M H_2SO_4 for comparison (**Figure 3**a,b). Pristine carbon paper that supports β-Mo_2C shows negligible activity in hydrogen evolution, and works as an inert conductive loading substrate in the system. The catalytic activities of electrode increase with the mass loading of Mo_2C, and the optimized mass loading is selected as 1 mg cm^{-2} (Figure S9a,b, Supporting Information). Tafel plots are fitted to the Tafel equation ($\eta = \beta \log(j) + \alpha$) to elucidate the HER mechanism and kinetic properties. With a mass loading of 1 mg cm^{-2} in an acidic environment (0.5 M H_2SO_4), Mo_2C provides a Tafel slope of 68 mV dec^{-1} (Figure S9a, Supporting Information).

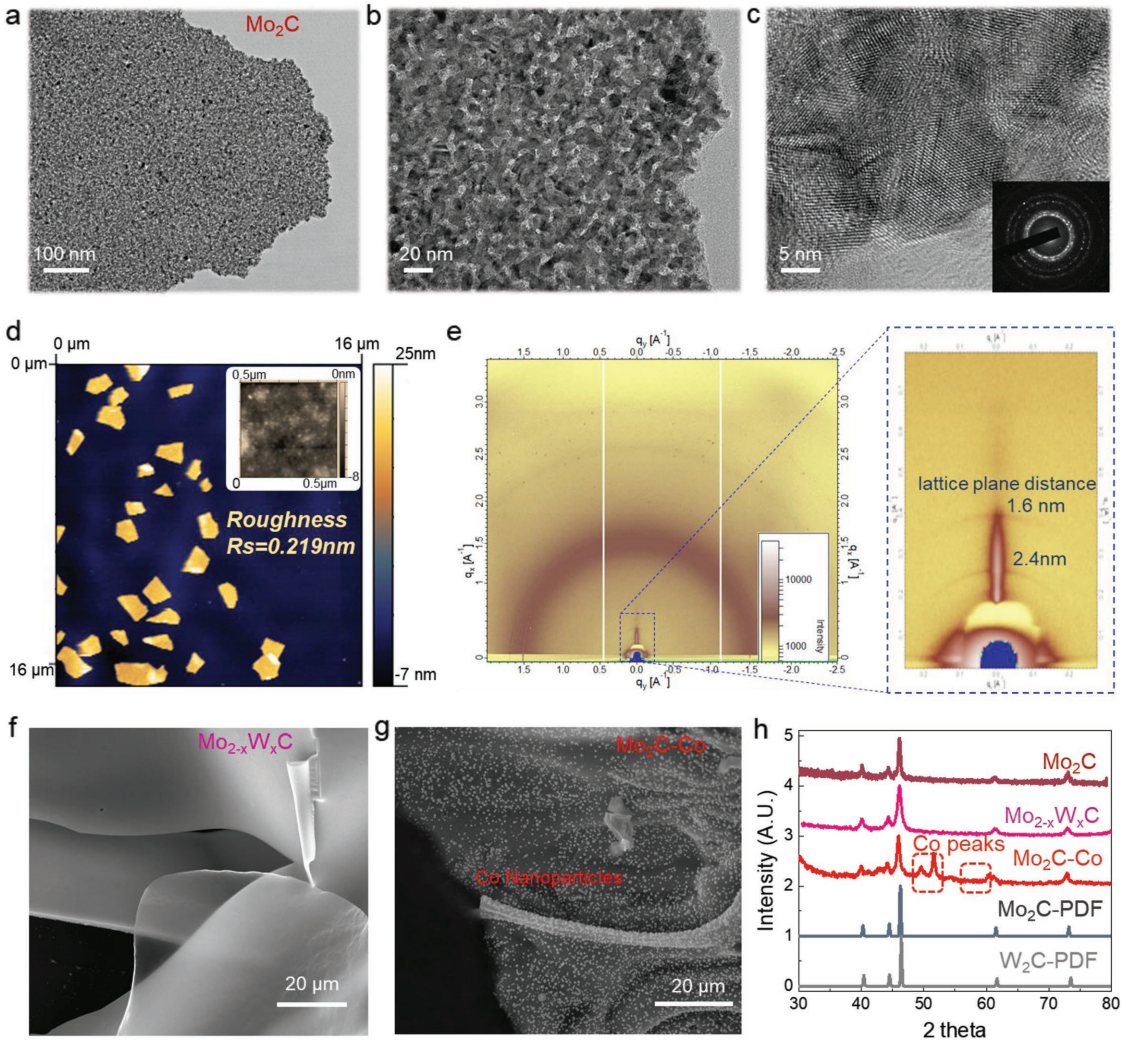

Figure 2. Characterizations of ultrathin Mo_2C and hybrid structure $Mo_{2-x}W_xC$ and Mo_2C–Co. a–c) TEM images revealing the micro-/nanoscale structures. d) AFM structural height mapping results showing a typical thickness of ≈10 nm and a surface roughness of ≈0.22 nm. e) GIWAX characterizations implying two sublayer thicknesses of 2.4 and 1.6 nm (Figure S4, Supporting Information). f) SEM image of the as-synthesized binary $Mo_{2-x}W_xC$ showing excellent ultrathin 2D structures. g) SEM image of the as-synthesized binary Mo_2C–Co showing ultrathin Mo_2C sheets deposited by Co nanoparticles. h) X-ray diffraction results of the as-synthesized 2D Mo_2C from a single metal–gelatin solution, and the as-synthesized binary $Mo_{2-x}W_xC$ and Mo_2C–Co structures from mixed metal ions and gelatin solutions.

Once decorated with Co nanoparticles, this hybrid structure enhances the HER responses with a low Tafel slope at 39 mV dec^{-1} and overpotential at 48 $mV_{j=10\,mA\,cm^{-2}}$ (Figure 3 and **Table 1**). Although the electrode made of $Mo_{2-x}W_xC$ does not provide a lower Tafel slope, it reduces the overpotential to 60 $mV_{j=10\,mA\,cm^{-2}}$. One hypothesis is that a low onset potential induced by the lattice strain in the intergrowth Mo–W matrix can induce high efficacy of catalytic reactions.[40,41] Electrochemical impedance spectroscopy (EIS) results in Figure 3c are fitted with the equivalent model in the inset to study the HER kinetics (Figure 3c).[42] Also, the values of series resistance (R_s) and charge transfer resistance (R_{ct}) calculated from the Nyquist plots are summarized in Table S1 (Supporting Information). R_{ct} of Mo_2C–Co and $Mo_{2-x}W_xC$ are both lower than that of Mo_2C, showing an improved HER efficiency. The R_{ct} and R_s values of Mo_2C–Co are surprisingly close to that of Pt/C, announcing the superior performance of Mo_2C–Co. Electrochemical surface area (ECSA) is tested by cyclic voltammetry in the non-HER regime, as shown in Figure S10 and Table S2 (Supporting Information),[43] in which Mo_2C shows higher ECSA than Mo_2C and $Mo_{2-x}W_xC$. On the other hand, Mo_2C has a larger Brunauer–Emmett–Teller (BET) surface area at ≈6.2 $m^2\ g^{-1}$ than that of Mo_2C–Co at ≈4.6 $m^2\ g^{-1}$, while other mechanisms could boost up the ECSA value for Mo_2C–Co. ESCA and BET relate to different mechanisms of adsorption and diffusion in liquid and gas phases.

Density functional simulations elucidate the synergistic effects of the incorporation of Co atoms onto Mo_2C, which will effectively decrease the absolute Gibbs free energy of hydrogen adsorption ($|\Delta G_{H^*}|$) on carbide surface. The thermodynamic diagram of HER is illustrated in Figure 3d, including initial ($H^+ + e^- + *$, where * denotes an active site), intermediate (H^*), and final states ($* + 1/2H_2$).[44] It is observed that β-Mo_2C

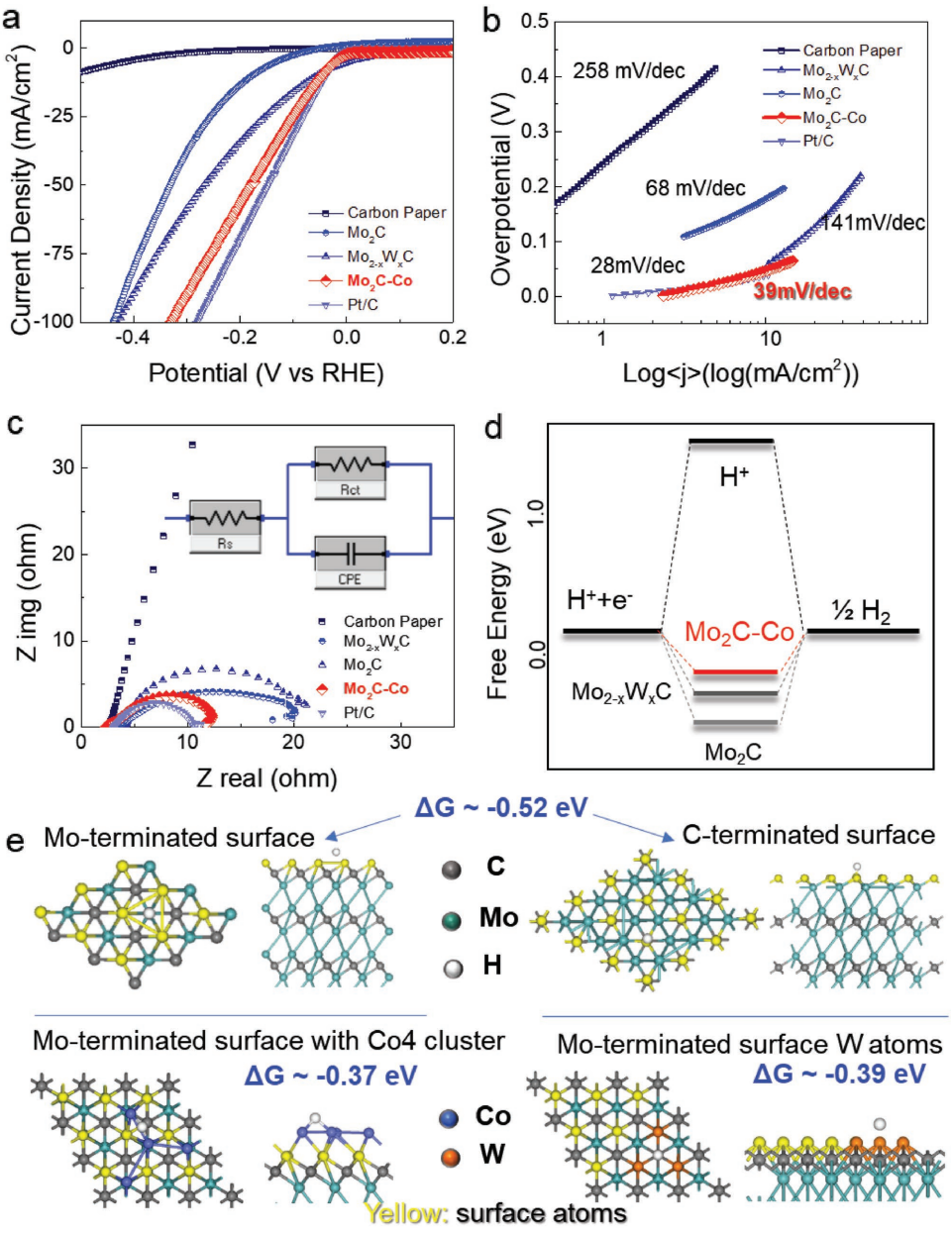

Figure 3. Performance of 2D Mo_2C and binary 2D carbides as HER catalysts in 0.5 M H_2SO_4. a) Linear sweep voltammetry of HER of different metal carbide materials. Mass loading is set as 1 mg cm^{-2}. The pristine carbon paper and carbon paper loaded with 1 mg cm^{-2} Pt/C are also tested for comparison. b) The corresponding Tafel slopes and overpotentials of the different active materials in (a). c) Electrochemical impedance spectroscopy (EIS) Nyquist plots of Mo_2C, Mo_2C–Co, and $Mo_{2-x}W_xC$, at $V_{dc} = -0.3$ V versus RHE. d) Calculated thermodynamic energy diagram for the HER activities of Mo_2C, Mo_2C–Co, and $Mo_{2-x}W_xC$. e) Side and top views of optimized Mo_2C, Mo_2C–Co, and $Mo_{2-x}W_xC$ with one adsorbed hydrogen atom. The free energies for hydrogen adsorption are calculated accordingly.

provides low $|\Delta G_{H^*}|$ of ≈0.52 eV, which is further reduced to 0.37 eV with the decoration of Co atoms (Figure 3e). Similarly, $Mo_{2-x}W_xC$ surface demonstrates a $|\Delta G_{H^*}|$ of 0.39 eV, close to that of the Mo_2C–Co case. More discussions are in Figures S11 and S12 (Supporting Information). Meanwhile, a stability test is shown in Figure S13 (Supporting Information), which shows stable performance of Mo_2C–Co during the 12 h hydrogen production at an overpotential of 0.4 V (Figure S11, Supporting Information). The potential leaching problem of Co is alleviated in the diluted acid with the relatively slow kinetics,[45] especially under the negative voltage during the HER test which suppresses the dissolution reaction.

The material performance can be attributed to several key properties, including high surface area due to the ultrathin structure, robust conjugation between Mo_2C and the rich carbon phase for high conductivity and electron transport, abundant grain boundaries that could perform as active center originating from nanocrystals, and the catalytic activity of the material lattice plane. Catalyst efficacy is particularly dependent on the lattice plane; for example, the activities of basal and edge

Table 1. Summary of catalyst activity of different carbides for HER in 0.5 M H_2SO_4.

	Tafel slope [mV dec^{-1}]	Overpotential [mV] @ j = 10 mA cm^{-2}
Carbon paper	258	589
Mo_2C	68	178
$Mo_{2-x}W_xC$	141	60
Mo_2C–Co	39	48
Pt/C	28	38

of chalcogenides and MXenes widely differ.[46,47] As a general rule, large single crystals or sheets have their lowest-energy surface exposed, and have a corresponding poor catalytic performance. However, defects and grain boundaries often present additional active sites by exposing more "preferred" catalytic crystalline faces. The random orientation of the ultrafine Mo_2C domains dispersed in the large 2D-TMC sheets provides a variety of such defective sites despite the flat nature of the nanosheets.

Leveraging the bottom-up self-assembly material design in the precursor-free method can help synthesize new phases, compositions, and heterostructures of 2D TMCs using a low-temperature manufacturing process. We have demonstrated that supramolecular order in metallohydrogels is conserved for the formation of ultrathin polycrystalline transition metal carbides, MC_x (M = Mo, W, Co). The gelatin-based precursor can assist the transition metal ions (Mo^{5+}, W^{6+}, Co^{2+}) to form layer-by-layer metal carbide nanocrystals at a relatively low temperature (600 °C). The role of gelatin and metal complex concentration was examined using the Mo–gelatin as a model system for optimizing conductivity, large lateral size, and high crystallinity. Through this method, binary/ternary carbides/hybrids such as Mo_2C–Co, $Mo_{2-x}W_xC$, and others can be produced in a single synthesis step. We also found that cobalt nanoparticles incidentally deposit onto the nanosheet structures if added to the precursor with the molybdenum or tungsten complexes. The products were homogenous, consisting of large, thin sheets comprised of randomly orientated metal carbide nanocrystals (<5 nm in size).

We then evaluated these materials for their HER activity and found that all of the MC_x (M = Mo, W, Co) and their binary structures can serve as HER catalysts. Among them, Mo_2C–Co provides the smallest Tafel slope of 39 mV dec^{-1} and the lowest overpotential of $48\ mV_{j=10\ mA\ cm^{-2}}$ (**Table 2**). The outstanding electrochemical catalysis performance is competitive with previous reported HER catalysts for a broad range of water hydrolysis and other energy-related applications.[48] Further study on the use of supramolecular order to precisely control the atomic positions of metal atoms in the carbide framework may reveal opportunities to further improve their stability and performance. The straightforward development of more elaborate functional metal carbides will also promote their applications in clean energy and environmental fields, including energy storage, catalysis, solar thermal energy harvesting, and harsh environment monitoring applications.[49]

Experimental Section

Preparation of Ion-Gelatin Solution: $MoCl_5$, $CoSO_4$ (all purchased from Sigma-Aldrich) were dissolved in DI water, and WCl_6 was dissolved in NMP with a concentration of 2 m (molal, mol kg^{-1} sol). The hydrogel was made by dissolving either gelatin, poly(vinylpyrrolidone) (PVP), or poly(ethylene oxide) (PEO) with 60 wt% stirred on a hot plate for 2 h at 80 °C.

Synthesis Process: 100 µL of ion–gel solutions were placed on a high-temperature resilient quartz boat (1 cm × 1.7 cm × 10 cm, MTI Corp.) and was loaded into a furnace (1 in. in diameter, Lindberg Thermal Furnace). The temperature was ramped up to 600 °C in 10 min under 30 sccm of H_2, and 10 sccm of CH_4 was added for 15 min at 600 °C. The furnace was rapidly cooled to room temperature and the 2D TMCs were separated from the quartz boats, ground, dispersed in DI water, sonicated for 30 min, vacuum filtrated, and dried overnight at 80 °C.

Material Characterization: SEM (FEI Quanta 3D) was employed to study the morphology and structure. Different carbides were dispersed in alcohol by sonication for 2 h, and dropped onto a copper grid (2 µm mesh size). The transmission electron microscopy (TEM) and high-resolution transmission electron microscopy (HRTEM) images were observed under a JEOL JEM-2100F field emission TEM (200 kV). XRD (Bruker D8) was performed to study the crystallinity, using Co as source (35 mV, 40 kV) for powder diffraction. X-ray photoelectron spectroscopy (CHI) was used to study the surface element component of samples. 2 mm Al monochromatic source was employed to first scan a 500–50 eV survey of wide range spectrum, followed with specific high-resolution Mo_3d, W_4f, and C_1s orbital scanning. AFM (Bruker Icon AFM) was employed to scan the thickness of carbide flakes and investigate the surface roughness. Dispersed carbide sheets on silicon wafer were picked under an optical microscope, and mapped with a silicon carbide tip at standard tapping mode.

GIWAX: GIWAXS spectra were taken at beamline 7.3.3. at the Advanced Light Source (ALS) at the Lawrence Berkeley National Lab utilizing an incident wavelength of 0.124 nm at 10 keV, with a pixel size of 0.172 mm. 2D spectra were recorded with a Pilatus 2M-2D detector and integrated to reduce to 1D with the NIKA GIWAXS software.

Table 2. Comparison of the catalyst activity of Mo_2C–Co with other HER materials.

HER in 0.5 M H_2SO_4	Tafel slope [mV dec^{-1}]	Overpotential [mV]@j = 10 mA cm^{-2}	Catalyst loading [mg cm^{-2}]	Exchange current j_0 [mA cm^{-2}]	Ref.
W_2C/multiwall carbon nanotubes (MWCNTs)	45	123	≈0.56	0.018	[50]
MoC_x nano-octahedrons	53	142	0.8	0.023	[51]
Mo_2C@N,P-codoped carbon shells (NPC)/N,P-codoped reduced graphene oxide (NPRGO)	33.6	34	0.14	1.09	[52]
2D-MoS_2 quantum dots (QDs)	44	92	0.1	0.042	[42]
Mo2C–Co	39	48	1.0	0.578	This work

Electrochemical Test for HER: Ag/AgCl was used as the reference electrode, while a carbon rod was used as the counter electrode to study the 2D TMCs in 0.5 M H_2SO_4. Linear sweep voltammetry, cyclic voltammetry, chronopotentiometry, and EIS impedance tests were performed by an electrochemistry workstation (Gamry Ref 600) with different modules. The polarization curves were obtained by sweeping the potential from 0 to –0.8 V versus Ag/AgCl at room temperature at a sweep rate of 10 mV s^{-1}. The EIS was performed from 100 kHz to 0.1 Hz. Washed and dried powdery 2D TMCs were ground with polyacrylonitrile (PAN) (1 wt%) dissolved in NMP (Sigma-Aldrich) as a binder, which was cast onto a hydrophobic carbon paper (Toray carbon paper 060, wet proofed).

Calibration of Reversible Hydrogen Electrode (RHE): The reference electrode was calibrated to RHE using a platinum electrode for both working and counter electrodes in the same electrolyte. The calibration resulted in a shift of –0.265 V versus the RHE in 0.5 M H_2SO_4.

Density Function Theory (DFT) Simulations: Using the Vienna Ab-initio Simulation Package (VASP[53]), all calculations were performed adopting the Perdew–Burke–Ernzerhof (PBE[54]) version of generalized gradient approximation with projector-augmented wave potentials.[55,56] A $3 \times 3 \times 1$ supercell of Mo_2C (001) slab with five layers of Mo_2C was chosen as the models, and the middle layer of Mo_2C was kept fixed to simulate the bulk. For Mo_2C–Co, a Co_4 cluster adsorbing on the surface was constructed, while for $Mo_{2-x}W_xC$, three nearest-neighbor Mo atoms were substituted by W atoms. To keep the spurious interactions negligible, a vacuum layer larger than 10 Å was selected. The force convergence criterion for structural optimization was set as 0.01 eV $Å^{-1}$. Following computational hydrogen electrode model,[57] the free energy of H^+ was obtained as $G(H^+) = 1/2G(H_2)$, assuming $2H^+ \rightarrow H_2$ was in equilibrium. Thermodynamic free energies of considered states were defined as $G = E_{DFT} + E_{ZPE} - TS$, where E_{DFT} and E_{ZPE} were DFT ground state energy and zero-point energy (ZPE) according to harmonic approximation with vibration frequencies obtained from DFT. The vibrational entropy for adsorbed species was calculated[58] as, $S = k_B\left[\sum_i \ln\left(\frac{1}{1-e^{-h\nu_i/k_BT}}\right) + \sum_i \frac{h\nu}{k_BT}\frac{1}{\left(e^{h\nu_i/k_BT}-1\right)} + 1\right]$ and the entropy for molecules was taken from the standard tables for gas-phase molecules.[57]

Supporting Information

Supporting Information is available from the Wiley Online Library or from the author.

Acknowledgements

X.Z., W.C., and X.Z. contributed equally to this work. The authors warmly thank the discussion with Prof. Gabor Somorjai and his group members in the UC Berkeley chemistry department. The theoretical part was supported by the Youth 1000-Talent Program of China, and the Development and Reform Commission of Shenzhen Municipality for the development of the "Low-Dimensional Materials and Devices" Discipline. The authors would like to thank Dr. C. Shen for discussion of the paper. Work at the Molecular Foundry was supported by the Office of Science, Office of Basic Energy Sciences, of the U.S. Department of Energy under Contract No. DE-AC02-05CH11231. Work at the Advanced Light Source was supported by the Office of Science, Office of Basic Energy Sciences, of the U.S. Department of Energy under Contract No. DE-AC02-05CH11231. Beamline 7.3.3 of the Advanced Light Source is supported by the Director of the Office of Science, Office of Basic Energy Sciences, of the U.S. Department of Energy under Contract No. DE-AC02-05CH11231.

Conflict of Interest

The authors declare no conflict of interest.

Keywords

2D transition metal carbide (2D TMC), hydrogen electrocatalysis., metallohydrogel, self-assembly

Received: August 9, 2018
Revised: September 14, 2018
Published online: October 9, 2018

[1] N. S. Lewis, D. G. Nocera, *Proc. Natl. Acad. Sci. USA* **2006**, *103*, 15729.
[2] M. G. Walter, E. L. Warren, J. R. McKone, S. W. Boettcher, Q. X. Mi, E. A. Santori, N. S. Lewis, *Chem. Rev.* **2010**, *110*, 6446.
[3] X. D. Yao, C. Z. Wu, A. J. Du, J. Zou, Z. H. Zhu, P. Wang, H. M. Cheng, S. Smith, G. Q. Lu, *J. Am. Chem. Soc.* **2007**, *129*, 15650.
[4] M. Z. Jacobson, W. G. Colella, D. M. Golden, *Science* **2005**, *308*, 1901.
[5] E. J. Popczun, J. R. McKone, C. G. Read, A. J. Biacchi, A. M. Wiltrout, N. S. Lewis, R. E. Schaak, *J. Am. Chem. Soc.* **2013**, *135*, 9267.
[6] C. C. L. McCrory, S. Jung, I. M. Ferrer, S. M. Chatman, J. C. Peters, T. F. Jaramillo, *J. Am. Chem. Soc.* **2015**, *137*, 4347.
[7] Z. W. Seh, K. D. Fredrickson, B. Anasori, J. Kibsgaard, A. L. Strickler, M. R. Lukatskaya, Y. Gogotsi, T. F. Jaramillo, A. Vojvodic, *ACS Energy Lett.* **2016**, *1*, 589.
[8] C. Xu, L. Wang, Z. Liu, L. Chen, J. Guo, N. Kang, X.-L. Ma, H.-M. Cheng, W. Ren, *Nat. Mater.* **2015**, *14*, 1135.
[9] H. S. Jang, B. Seong, X. Zang, H. Lee, J. W. Bae, D. H. Cho, E. Kao, C. Yang, G. Kang, Y. Liu, H. S. Park, D. Byun, L. Lin, *Adv. Mater. Interfaces* **2018**, *5*, 1701491.
[10] G. R. Bhimanapati, Z. Lin, V. Meunier, Y. Jung, J. Cha, S. Das, D. Xiao, Y. Son, M. S. Strano, V. R. Cooper, L. B. Liang, S. G. Louie, E. Ringe, W. Zhou, S. S. Kim, R. R. Naik, B. G. Sumpter, H. Terrones, F. N. Xia, Y. L. Wang, J. Zhu, D. Akinwande, N. Alem, J. A. Schuller, R. E. Schaak, M. Terrones, J. A. Robinson, *ACS Nano* **2015**, *9*, 11509.
[11] D. S. Kong, J. J. Cha, H. T. Wang, H. R. Lee, Y. Cui, *Energy Environ. Sci.* **2013**, *6*, 3553.
[12] C. Kastl, C. T. Chen, T. Kuykendall, B. Shevitski, T. P. Darlington, N. J. Borys, A. Krayev, P. J. Schuck, S. Aloni, A. M. Schwartzberg, *2D Mater.* **2017**, *4*, 021024.
[13] Z. Q. Sun, T. Liao, Y. H. Dou, S. M. Hwang, M. S. Park, L. Jiang, J. H. Kim, S. X. Dou, *Nat. Commun.* **2014**, *5*, 3818.
[14] L. L. Peng, P. Xiong, L. Ma, Y. F. Yuan, Y. Zhu, D. H. Chen, X. Y. Luo, J. Lu, K. Amine, G. H. Yu, *Nat. Commun.* **2017**, *8*, 15139.
[15] Q. Tao, M. Dahlqvist, J. Lu, S. Kota, R. Meshkian, J. Halim, J. Palisaitis, L. Hultman, M. W. Barsoum, P. O. Persson, *Nat. Commun.* **2017**, *8*, 14949.
[16] R. Meshkian, M. Dahlqvist, J. Lu, B. Wickman, J. Halim, J. Thörnberg, Q. Tao, S. Li, S. Intikhab, J. Snyder, W. Barsoum Michel, M. Yildizhan, J. Palisaitis, L. Hultman, O. Å. Persson Per, J. Rosen, *Adv. Mater.* **2018**, *30*, 1706409.
[17] X. N. Zang, C. W. Shen, Y. Chu, B. X. Li, M. S. Wei, J. W. Zhong, M. Sanghadasa, L. W. Lin, *Adv. Mater.* **2018**, *30*, 1800062.
[18] M. Ghidiu, M. R. Lukatskaya, M. Q. Zhao, Y. Gogotsi, M. W. Barsoum, *Nature* **2014**, *516*, 78.
[19] B. Anasori, M. R. Lukatskaya, Y. Gogotsi, *Nat. Rev. Mater.* **2017**, *2*, 16098.
[20] M. W. Barsoum, *Prog. Solid State Chem.* **2000**, *28*, 201.
[21] M. R. Lukatskaya, O. Mashtalir, C. E. Ren, Y. Dall'Agnese, P. Rozier, P. L. Taberna, M. Naguib, P. Simon, M. W. Barsoum, Y. Gogotsi, *Science* **2013**, *341*, 1502.
[22] P. Eklund, J. Rosen, P. O. Å. Persson, *J. Phys. D: Appl. Phys.* **2017**, *50*, 113001.

[23] H. Fashandi, M. Dahlqvist, J. Lu, J. Palisaitis, S. I. Simak, I. A. Abrikosov, J. Rosen, L. Hultman, M. Andersson, A. L. Spetz, *Nat. Mater.* **2017**, *16*, 814.
[24] Y. Gogotsi, *Nat. Mater.* **2015**, *14*, 1079.
[25] D. C. Geng, X. X. Zhao, Z. X. Chen, W. W. Sun, W. Fu, J. Y. Chen, W. Liu, W. Zhou, K. P. Loh, *Adv. Mater.* **2017**, *29*, 1700072.
[26] A. L. Lehninger, *Physiol. Rev.* **1950**, *30*, 393.
[27] M. Reches, E. Gazit, *Science* **2003**, *300*, 625.
[28] M. C. Daniel, D. Astruc, *Chem. Rev.* **2004**, *104*, 293.
[29] S. Mann, *Nat. Mater.* **2009**, *8*, 781.
[30] H. Hu, R. G. Larson, *Langmuir* **2005**, *21*, 3972.
[31] D. Villers, J. K. Platten, *J. Fluid Mech.* **1992**, *234*, 487.
[32] F. Wang, J. H. Seo, G. F. Luo, M. B. Starr, Z. D. Li, D. L. Geng, X. Yin, S. Y. Wang, D. G. Fraser, D. Morgan, Z. Q. Ma, X. D. Wang, *Nat. Commun.* **2016**, *7*, 10444.
[33] H. Yan, J. N. Hohman, F. H. Li, C. J. Jia, D. Solis-Ibarra, B. Wu, J. E. P. Dahl, R. M. K. Carlson, B. A. Tkachenko, A. A. Fokin, P. R. Schreiner, A. Vailionis, T. R. Kim, T. P. Devereaux, Z. X. Shen, N. A. Melosh, *Nat. Mater.* **2017**, *16*, 349.
[34] S. L. Cumberland, K. M. Hanif, A. Javier, G. A. Khitrov, G. F. Strouse, S. M. Woessner, C. S. Yun, *Chem. Mater.* **2002**, *14*, 1576.
[35] O. V. Mikhailov, *J. Coord. Chem.* **2008**, *61*, 1333.
[36] O. V. Mikhailov, *Nano Rev.* **2014**, *5*, 21485.
[37] B. Macias, J. J. Criado, M. V. Vaquero, M. V. Villa, *Thermochim. Acta* **1993**, *223*, 213.
[38] A. L. Patterson, *Phys. Rev.* **1939**, *56*, 978.
[39] G. G. Allan, *Tappi J.* **1997**, *80*, 262.
[40] H. W. Huang, H. H. Jia, Z. Liu, P. F. Gao, J. T. Zhao, Z. L. Luo, J. L. Yang, J. Zeng, *Angew. Chem., Int. Ed.* **2017**, *56*, 3594.
[41] P. P. Lopes, D. Strmcnik, D. Tripkovic, J. G. Connell, V. Stamenkovic, N. M. Markovic, *ACS Catal.* **2016**, *6*, 2536.
[42] W. Chen, J. Gu, Q. Liu, R. Luo, L. Yao, B. Sun, W. Zhang, H. Su, B. Chen, P. Liu, D. Zhang, *ACS Nano* **2018**, *12*, 308.
[43] Y. Huang, Q. F. Gong, X. N. Song, K. Feng, K. Q. Nie, F. P. Zhao, Y. Y. Wang, M. Zeng, J. Zhong, Y. G. Li, *ACS Nano* **2016**, *10*, 11337.
[44] E. Skulason, G. S. Karlberg, J. Rossmeisl, T. Bligaard, J. Greeley, H. Jonsson, J. K. Norskov, *Phys. Chem. Chem. Phys.* **2007**, *9*, 3241.
[45] K. N. Han, F. Lawson, *J. Less-Common Met.* **1974**, *38*, 19.
[46] D. S. Kong, H. T. Wang, J. J. Cha, M. Pasta, K. J. Koski, J. Yao, Y. Cui, *Nano Lett.* **2013**, *13*, 1341.
[47] A. D. Handoko, K. D. Fredrickson, B. Anasori, K. W. Convey, L. R. Johnson, Y. Gogotsi, A. Vojvodic, Z. W. Seh, *ACS Appl. Energy Mater.* **2018**, *1*, 173.
[48] P. Xiao, X. M. Ge, H. B. Wang, Z. L. Liu, A. Fisher, X. Wang, *Adv. Funct. Mater.* **2015**, *25*, 1520.
[49] P. Xiao, Y. Yan, X. M. Ge, Z. L. Liu, J. Y. Wang, X. Wang, *Appl. Catal., B* **2014**, *154–155*, 232.
[50] Q. F. Gong, Y. Wang, Q. Hu, J. G. Zhou, R. F. Feng, P. N. Duchesne, P. Zhang, F. J. Chen, N. Han, Y. F. Li, C. H. Jin, Y. G. Li, S. T. Lee, *Nat. Commun.* **2016**, *7*, 13216.
[51] H. B. Wu, B. Y. Xia, L. Yu, X. Y. Yu, X. W. Lou, *Nat. Commun.* **2015**, *6*, 6512.
[52] J. S. Li, Y. Wang, C. H. Liu, S. L. Li, Y. G. Wang, L. Z. Dong, Z. H. Dai, Y. F. Li, Y. Q. Lan, *Nat. Commun.* **2016**, *7*, 11204.
[53] G. Kresse, J. Furthmuller, *Phys. Rev. B* **1996**, *54*, 11169.
[54] J. P. Perdew, K. Burke, M. Ernzerhof, *Phys. Rev. Lett.* **1996**, *77*, 3865.
[55] G. Kresse, D. Joubert, *Phys. Rev. B* **1999**, *59*, 1758.
[56] P. E. Blochl, *Phys. Rev. B* **1994**, *50*, 17953.
[57] J. K. Norskov, J. Rossmeisl, A. Logadottir, L. Lindqvist, J. R. Kitchin, T. Bligaard, H. Jonsson, *J. Phys. Chem. B* **2004**, *108*, 17886.
[58] X. Zou, L. Wang, B. I. Yakobson, *Nanoscale* **2018**, *10*, 1129.